$[N(CH_3)_4]_2MnCl_4$

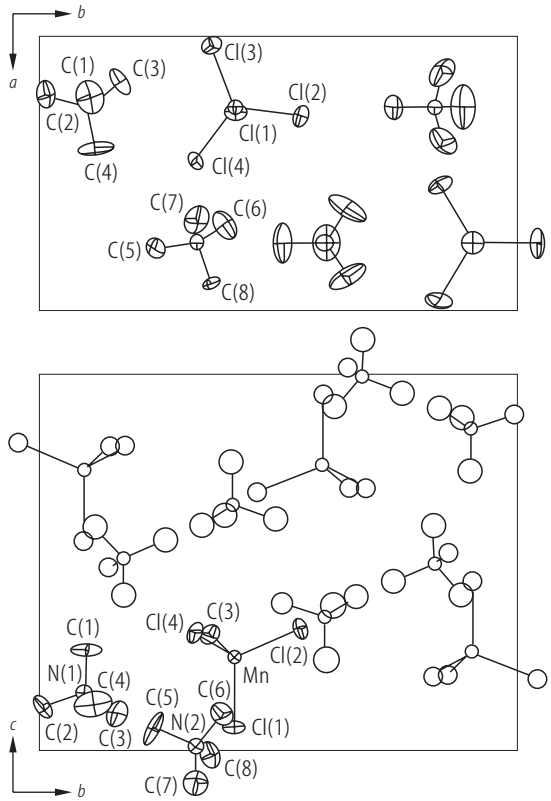

Fig. 39A-4-001. $[N(CH_3)_4]_2MnCl_4$. Structure of phase I [89Mas]. Projection along the *c* and *a* axes. $T = 293$ K. In the *a*-projection independent atoms are shown by thermal ellipsoids and other atoms by spheres. Configurations related by mirror reflection are not drawn.

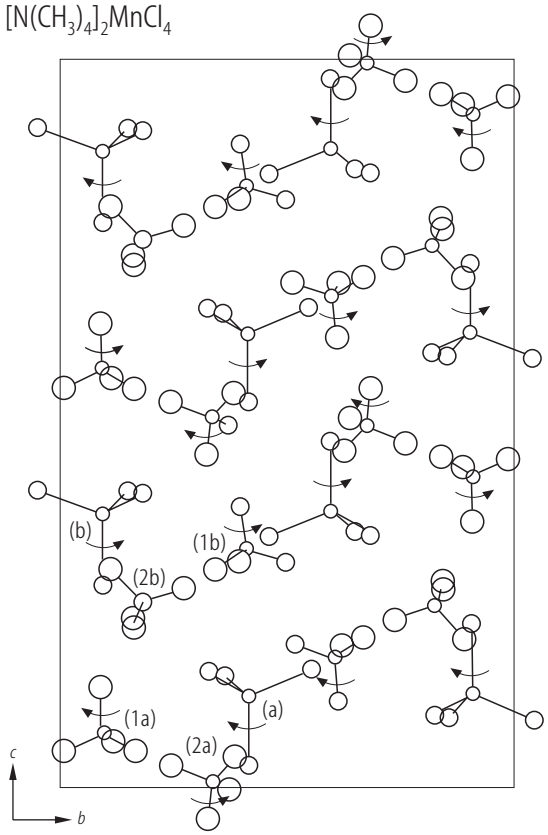

Fig. 39A-4-002. $[N(CH_3)_4]_2MnCl_4$. Structure of phase III [89Mas]. Projection along the *a* axis. $T = 273$ K. Rotations of ions about the *c* axis are indicated by arrows.

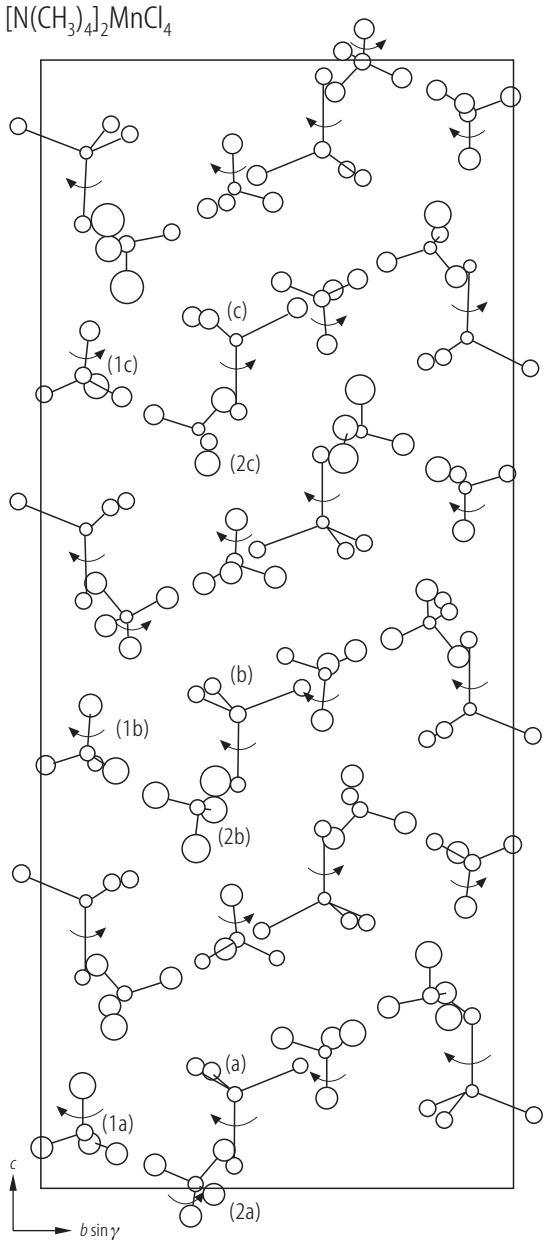

Fig. 39A-4-003. $[N(CH_3)_4]_2MnCl_4$. Structure of phase IV [89Mas]. Projection along the *a* axis. $T = 261$ K. Rotations of ions about the *c* axis are indicated by arrows.

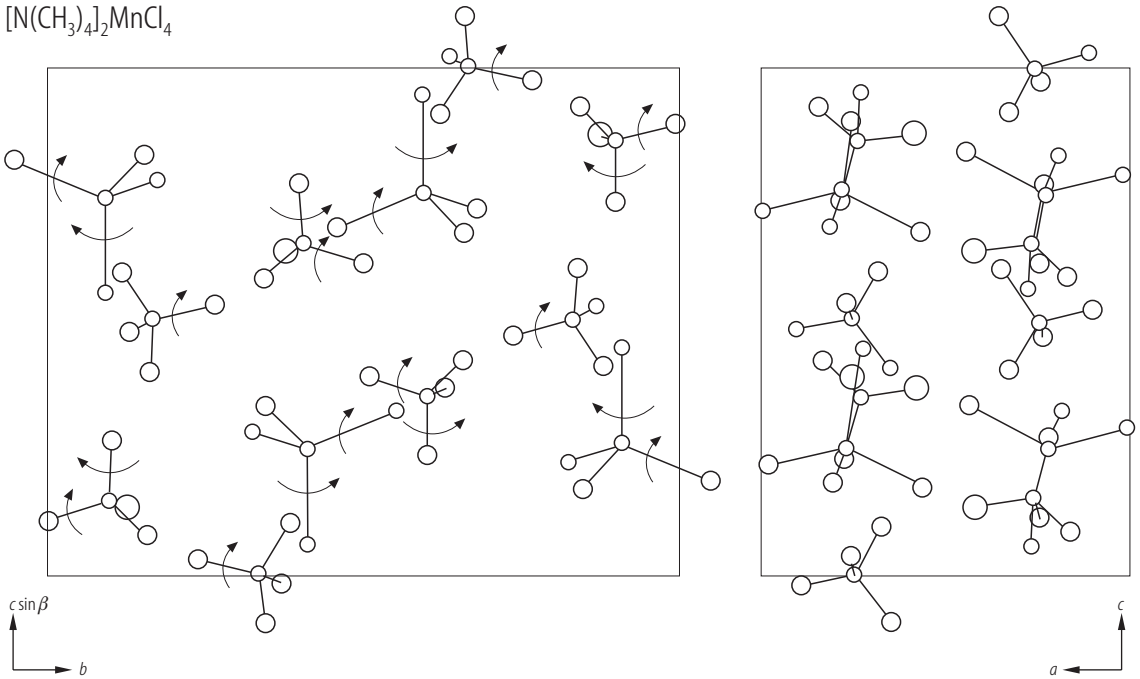

Fig. 39A-4-004. $[N(CH_3)_4]_2MnCl_4$. Structure of phase V [89Mas]. Projection along the *a* and *b* axes. T = 168 K. Rotations of the tetrahedra about the *b* and *c* axes are indicated by arrows.

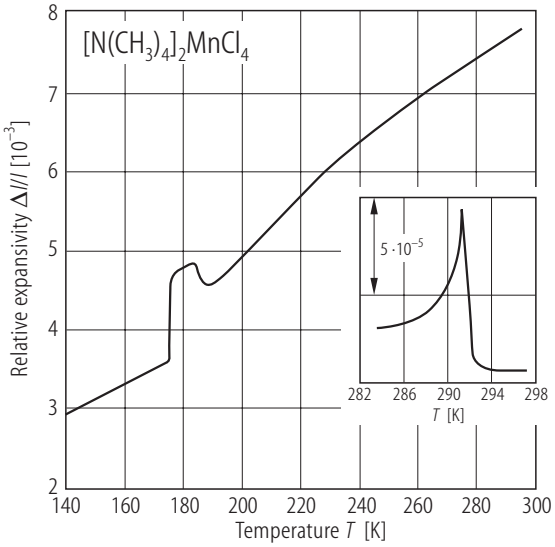

Fig. 39A-4-005. $[N(CH_3)_4]_2MnCl_4$. $\Delta l//l$ vs. T [90Kah]. $\Delta l//l$: linear thermal expansion along the *c* axis.

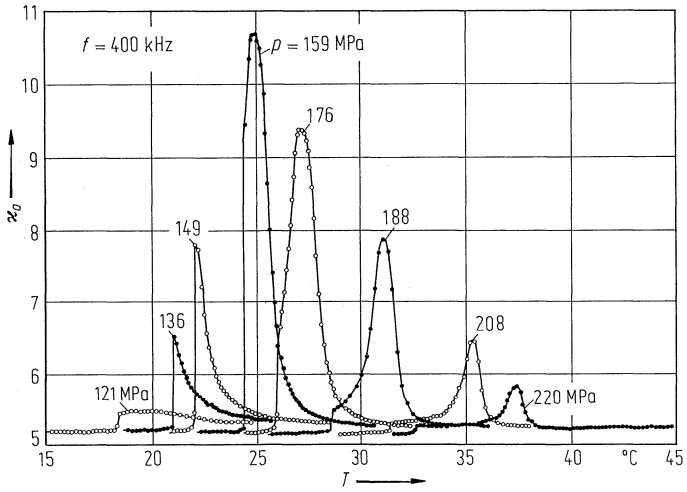

Fig. 39A-4-006. $[N(CH_3)_4]_2MnCl_4$. κ_a vs. T [84Ges]. Parameter: p.

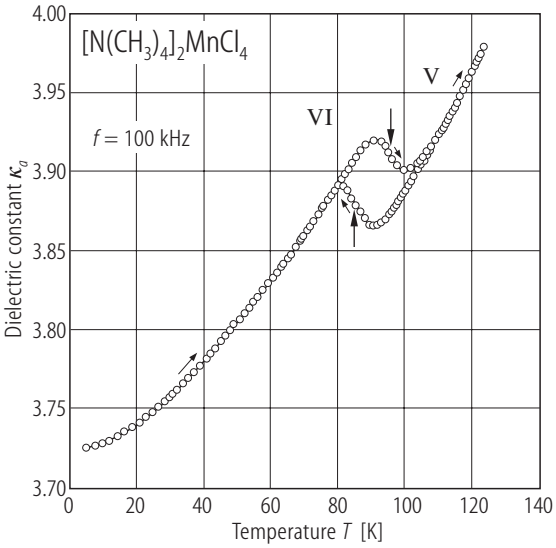

Fig. 39A-4-007. $[N(CH_3)_4]_2MnCl_4$. κ_a vs. T [89Ges].

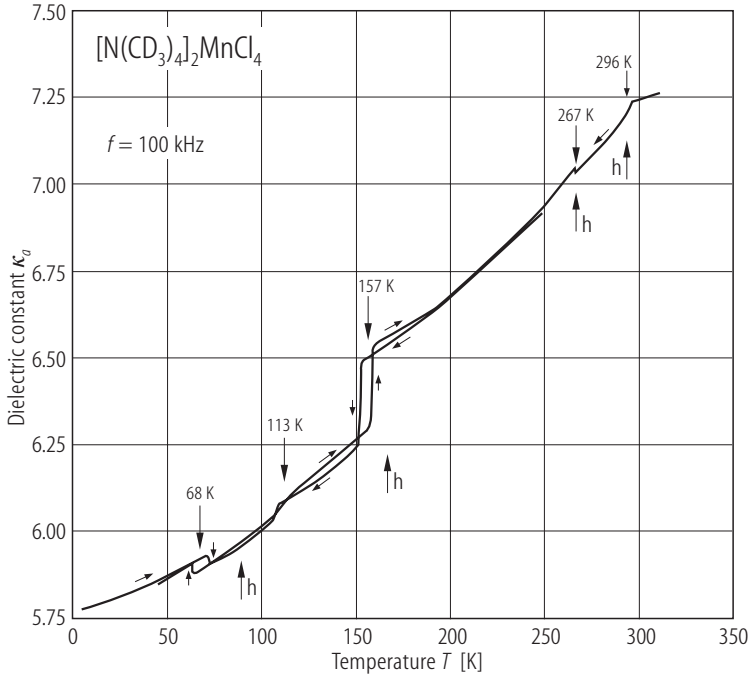

Fig. 39A-4-008. $[N(CD_3)_4]_2MnCl_4$. κ_a vs. T [89Ges]. Transition temperatures are shown by arrows. Phase transitions in $[N(CH_3)_4]_2MnCl_4$ are shown by upward-pointing arrows with 'h'.

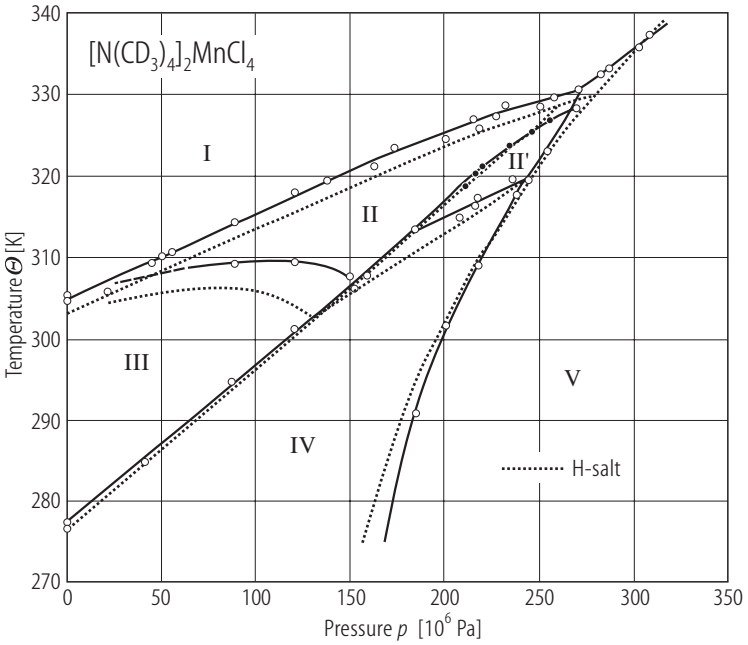

Fig. 39A-4-009. $[N(CD_3)_4]_2MnCl_4$. Θ vs. p [90Ges]. The phase boundaries of the deuterated compound and hydrogen one are indicated by solid and dotted lines, respectively. Full circle: position of dielectric constant peak.

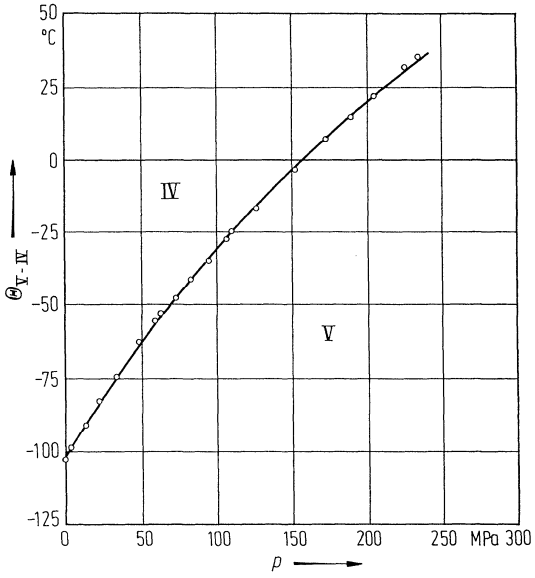

Fig. 39A-4-010. $[N(CH_3)_4]_2MnCl_4$. Θ_{V-IV} vs. p [84Ges].

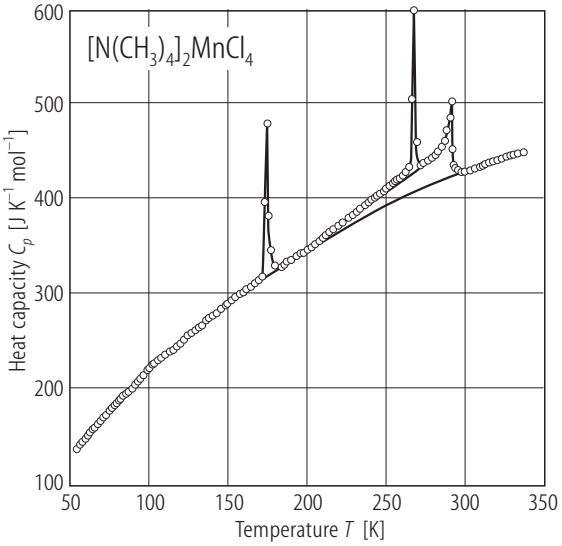

Fig. 39A-4-011. $[N(CH_3)_4]_2MnCl_4$. C_p vs. T [88Zub]. C_p: molar heat capacity at constant pressure.

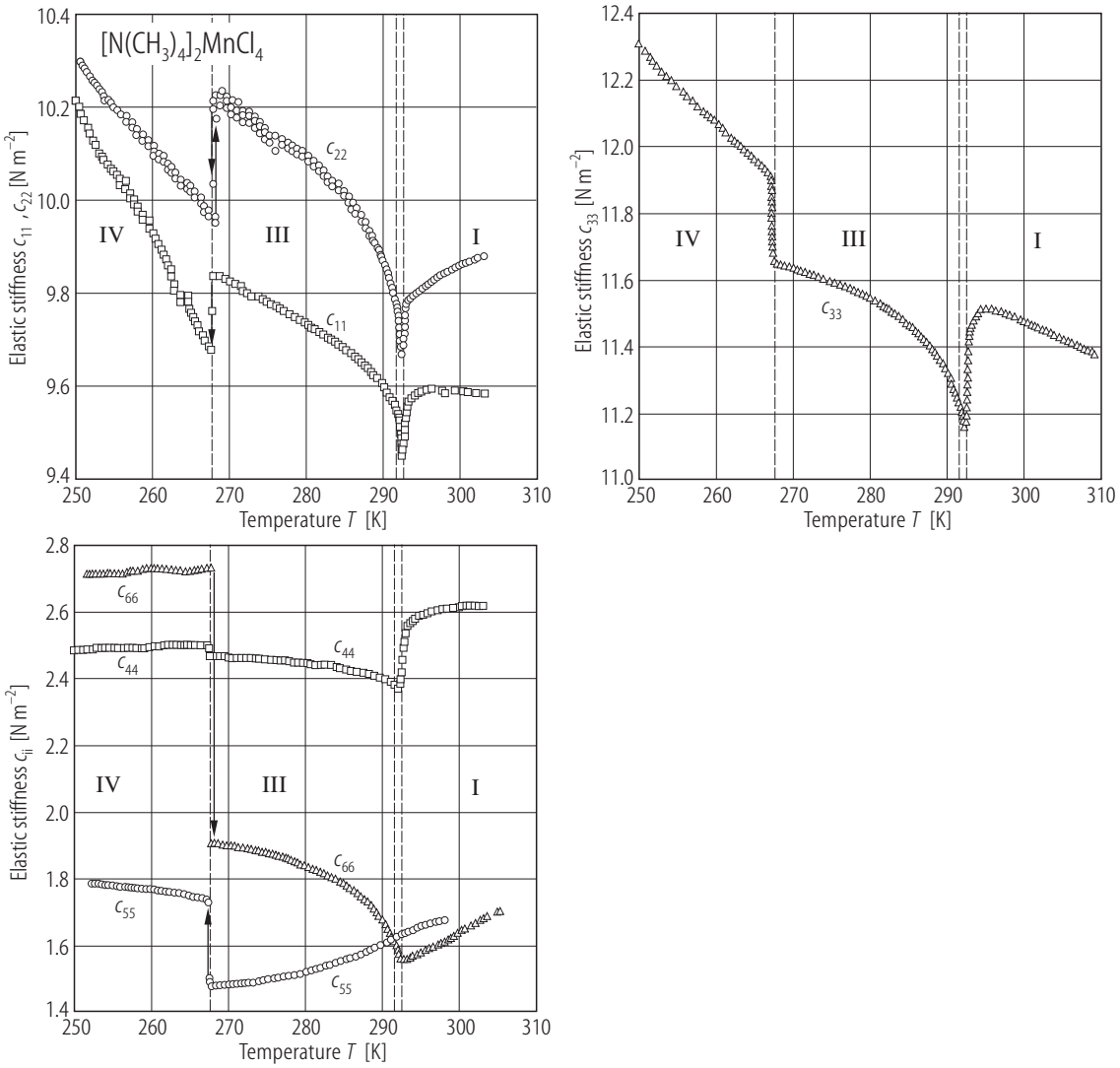

Fig. 39A-4-012. $[N(CH_3)_4]_2MnCl_4$. c_{ii} (i = 1 ... 6) vs. T [94Kub]. c_{ii}: elastic stiffness. f = 15 MHz.

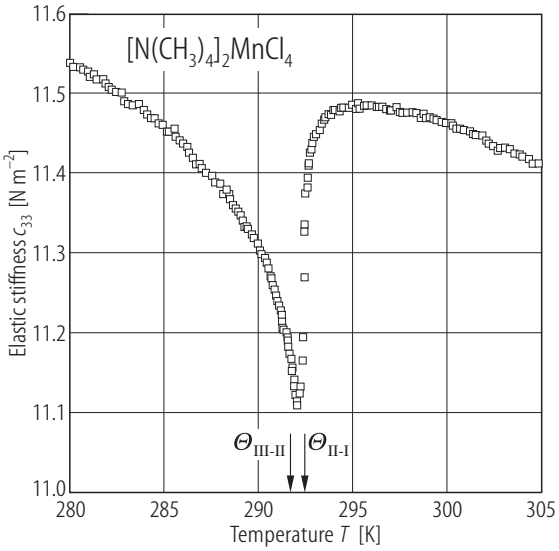

Fig. 39A-4-013. $[N(CH_3)_4]_2MnCl_4$. c_{33} vs. T near Θ_{II-I} [94Kub]. f = 12.7 MHz.

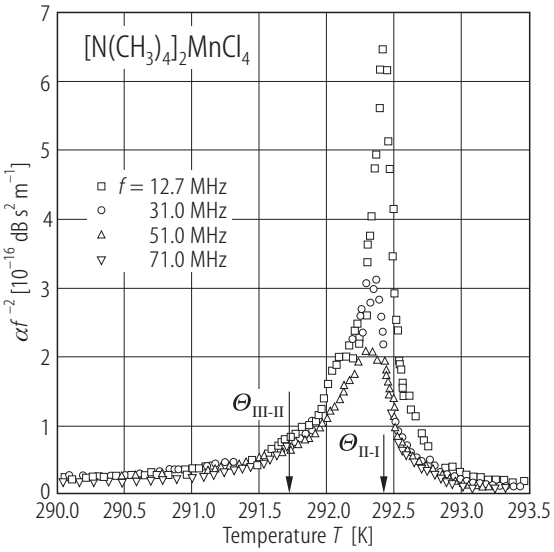

Fig. 39A-4-014. $[N(CH_3)_4]_2MnCl_4$. α/f^2 vs. T near Θ_{II-I} [94Kub]. α: acoustic absorption coefficient for a longitudinal wave propagating along the c axis. Parameter: f. Constant backgrounds are subtracted.

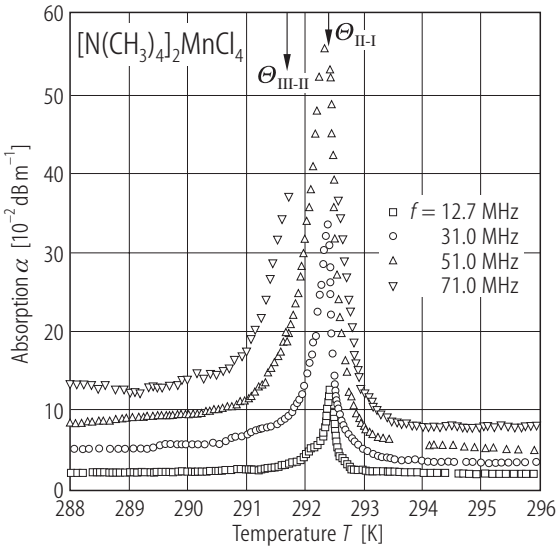

Fig. 39A-4-015. $[N(CH_3)_4]_2MnCl_4$. α vs. T near Θ_{II-I} [94Kub]. α: acoustic absorption coefficient for a longitudinal wave propagating along the c axis. Parameter: f.

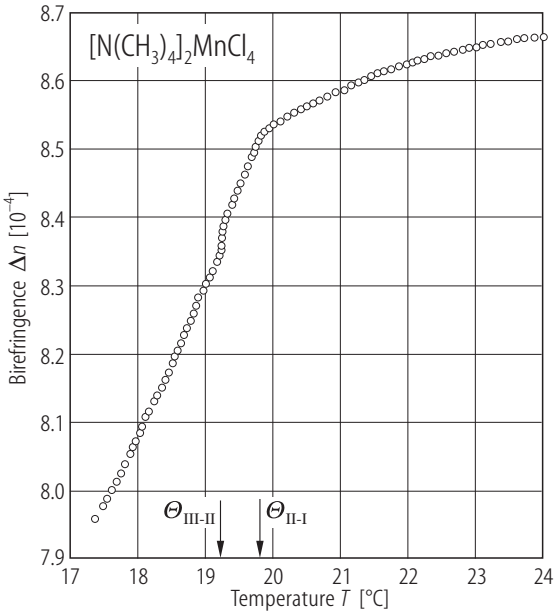

Fig. 39A-4-016. $[N(CH_3)_4]_2MnCl_4$. Δn vs. T [90Fui]. Δn: birefringence of light propagating along the b axis.

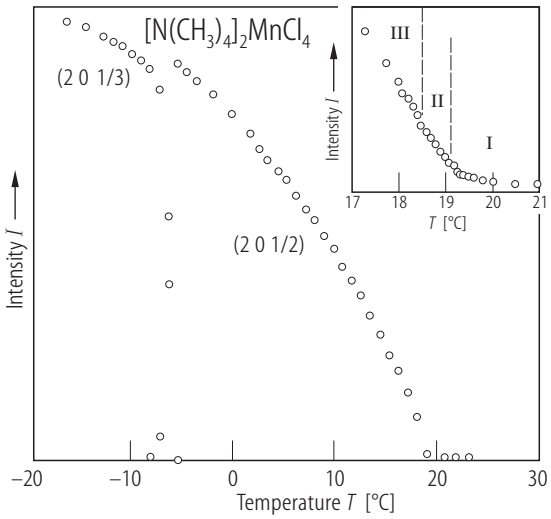

Fig. 39A-4-017. $[N(CH_3)_4]_2MnCl_4$. *I* vs. *T* [81Mas]. *I*: integrated intensities of X-ray reflections at (2, 0, ζ). ζ: modulation wavenumber in unit of c^*. The insert shows the intensities of the incommensurate reflection with $\zeta \approx 0.483$. The residual intensity in phase I is due to diffuse scattering.

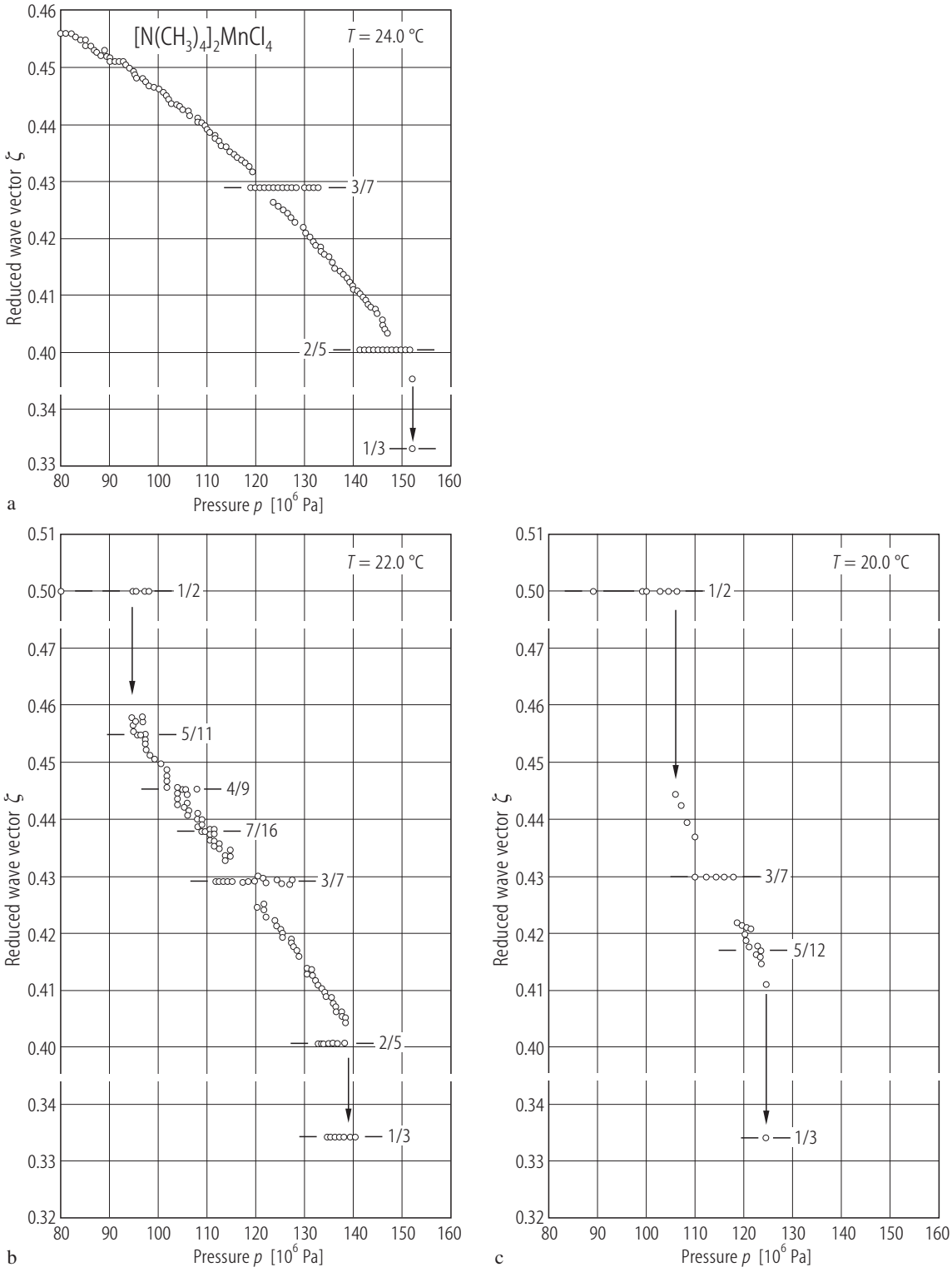

Fig. 39A-4-018. $[N(CH_3)_4]_2MnCl_4$. ζ vs. p [91Ham]. ζ: modulation wavenumber in unit of c^*. X-ray diffraction. (**a**) $T = 24.0$ °C, (**b**) $T = 22.0$ °C, (**c**) $T = 20.0$ °C.

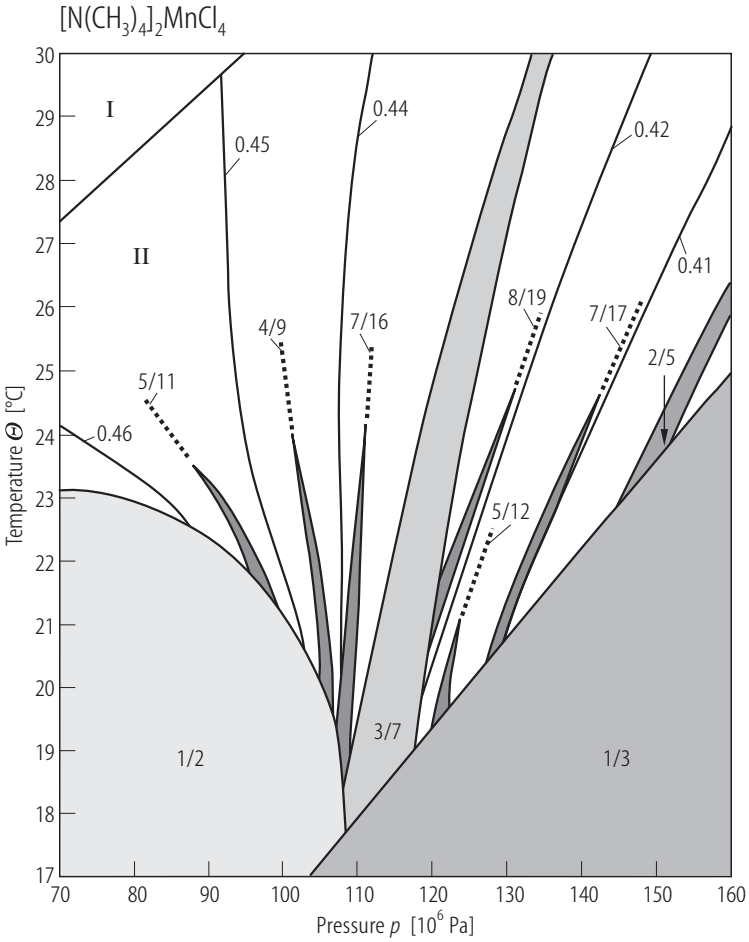

Fig. 39A-4-019. $[N(CH_3)_4]_2MnCl_4$. Θ vs. p [96Shi2]. X-ray diffraction. Gray areas show the commensurate phases, with corresponding modulation wavenumber in unit of c^*. The thin lines show contour lines of equal modulation wavenumber in the incommensurate area.